J Mater Sci (2007) 42:4110–4114
DOI 10.1007/s10853-006-0876-z

Study of preparation and magnetic properties of silica-coated cobalt ferrite nanocomposites

Lijun Zhao · Hua Yang · Yuming Cui · Xueping Zhao · Shouhua Feng

Received: 17 February 2005 / Accepted: 23 November 2005 / Published online: 21 April 2007

Abstract The structure and the magnetic properties of silica-coated cobalt ferrite nanoparticles (80 wt% $CoFe_2O_4$), prepared by sol–gel method and submitted to thermal treatments in the range 800–1,000 °C, were investigated through XRD, FT-IR, TEM and VSM. The effects of thermal treatment temperatures on the structure and magnetic properties of nanoparticles were examined. A silica shell thickness of about 5 nm was synthesized on top of cobalt ferrite nanoparticles. The non-crystalline silica confines the growth of cobalt ferrite nanoparticles, i.e., the particle sizes are almost independent of the thermal treatment. Saturation magnetization (Ms) was decreased slightly and coercivity (Hc) was increased, when the non-crystalline silica was coated on the surface of cobalt ferrite nanoparticles.

Introduction

Recently, many researchers have been active in preparing systems in which magnetic nanocrystalline particles grains are separated by means of a non-magnetic material in order to improve the magnetic properties, e.g., to obtain an increase of the coercivity. Of these non-magnetic materials (e.g., Al_2O_3, SiO_2, etc.), SiO_2 was observed to serve the purpose more favorably than its counterparts [1]. The advantages of silica are: exceptional stability of aqueous dispersions; easy surface modification that allows the preparation of non-aqueous colloids; easy control of interparticle interactions, both in solution and within structures, through shell thickness. Previous works involved the coating of hematite (Fe_2O_3) spindles [2], which could be subsequently reduced to metallic iron in a dry state [3], and much smaller magnetite (Fe_3O_4) clusters [4]. In such cases, coating was performed on an oxide, which easily binds to silica through OH surface groups.

Much of the current activities in the design and manufacturing of magnets is to enhance this parameter due to the increased need for permanent information storage [5, 6]. Spinel ferrite nanoparticles have been intensively investigated in recent years because of their remarkable electrical and magnetic properties and wide practical applications in information storage system, ferrofluid technology, magnetocaloric refrigeration and medical diagnosis. Among spinel ferrites, cobalt ferrite, $CoFe_2O_4$ is especially interesting because of its high cubic magnetocrystalline anisotropy, high coercivity and moderate saturation magnetization. $CoFe_2O_4$ is usually formed as an inverse spinel with the moment of the tetrahedral ions (Fe^{3+}) aligned anti-parallel to those of the octahedral ions (Co^{2+} and Fe^{3+}) and the resultant saturation moment is that of the cobalt ion amounting to 2–3 μ_B ($1\ \mu_B = 9.3 \times 10^{-24}\ JT^{-1}$) [7]. However, in some cases it has been found that Co^{2+} is present partially in both tetrahedral and octahedral sites [8]. These studies have been performed on samples prepared by several chemical

L. Zhao · H. Yang (✉) · Y. Cui
College of Chemistry, Jilin University,
Changchun 130023, P.R. China
e-mail: huayang86@vip.sina.com

X. Zhao
College of Physics, Jilin University,
Changchun 130023, P.R. China

S. Feng
State Key Laboratory of Inorganic Synthesis and Prepartive Chemistry, Jilin University, Changchun 130023, P.R. China

or physical processes and in most cases they are contained within a matrix. Amorphous silica is a well through matrix as a consequence of the considerable knowledge of its preparation by the sol–gel technique.

In this paper, we present the synthesis, characterization and magnetic properties of the materials consisting of 20 wt% silica-coated 80 wt% fraction of $CoFe_2O_4$ ferrite nanocrystal. It is expected that the high energetic product. The high coercivity is driven by the large anisotropy of the cobalt ion due to its important spin-orbit coupling. And the effects of thermal treatment on the magnetic parameter were carefully investigated.

Experimental

Cobalt ferrite nanocrystalline powders were obtained by emulsion method of nitrates dissolved in distilled water, PEG-20000 as a surfactant, maintaining the molar proportion cobalt and iron equal to 1:2. 2 M NH_4OH was dropped into the solution until Ph = 9.0 to form the suspension. The suspension was aged at 90 °C for 3 h, then centrifuged, washed with distilled water and ethanol to reduce agglomeration. The separated solid phase was dried at 90 °C for 7 h, and then the powder obtained was calcined at 800 °C in air atmosphere for 2 h.

The powder of $CoFe_2O_4$ (0.4 g) nanoparticles and tetraethyl orthosilicate (TEOS, 0.35 g) was dissolved in 50 mL of ethanol and formamide (0.07 g). The suspension was stirred for 3 h at room temperature and accompanied by the volatilization of ethanol. And then, water (0.15 g) acidified with nitric acid (0.002 g) as a catalyst was added. After gelation (approximately 2 h at 40 °C) and aging (24 h), the sample was dried at 150 °C for 1 day in air, and then it was calcined at 800, 900 and 1,000 °C in air (rate 10 °C min^{-1}) for 2 h, respectively.

The structure and the crystallite sizes were tested by X-ray diffractometer in the 2θ range 25–65° using CuKα radiation ($\lambda = 0.15405$ nm). The type of X-ray diffractometer is SHIMADZU Co.Tokyo Japan. The database of the Joint Committee on Powder Diffraction Data was used for the interpretation of XRD spectra. The crystallite sizes are calculated using Scherrer's relationship $D = k\lambda/B\cos\theta$, where 'D' is the average diameter in nm, 'k' is the shape factor, 'B' is the broadening of the diffraction line measured half of its maximum intensity in 'radians', 'λ' is the wave length of X-ray and 'θ' is the Bragg's diffraction angle. The crystallite sizes of the samples are estimated from the line width of the (311) XRD peaks. The particle size was estimated by XRD as well as by a Hitactli H-800 transmission electron microscope. For this measurement, the sample was deposited on copper grids and the microscope was operated at an accelerating potential of 175 KV. Mid-infrared spectra were recorded using a Nicolet-510 IR spectrometer on samples palletizing with KBr. Magnetic measurements are carried out at room temperature using a vibrating sample magnetometer (VSM) (Digital Measurement System JDM-13) with a maximum magnetic field of 10000 Oe.

Results and discussion

The powder X-ray diffraction pattern (Fig. 1) is characterized by a series of Bragg reflections corresponding closely to the $CoFe_2O_4$ ferrite. The silica is clearly non-crystalline but short-range correlation results in a very broad peak centered at a low two theta value of 22.5°, even if it is calcined at 1,000 °C. The partial crystallization of the silica manifested only for the sample heated up to 1,100 °C [9]. The diffraction patterns of phases other than silica exhibit broad peaks that become slightly sharper with the increasing temperature of the heat treatment. This corresponds well to crystal growth and complete crystallization.

The crystallite sizes estimated by XRD are listed in Table 1. It is clearly shows that the crystallite sizes of $CoFe_2O_4$ ferrite have a significant increase with the calcination temperatures. However, the crystallite sizes of silica-coated $CoFe_2O_4$ ferrite are almost independent of the calcination temperatures. This may be deduced that a well-established silica network provides a more effective confinement to the growth of $CoFe_2O_4$ particles.

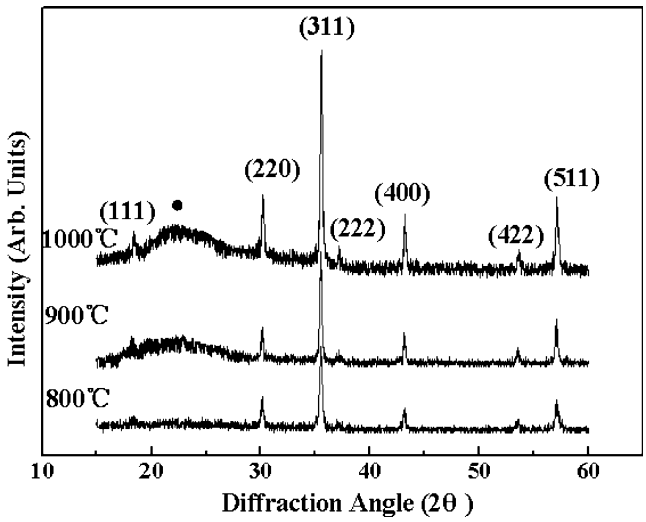

Fig. 1 XRD spectra for silica-coated $CoFe_2O_4$ nanocomposite treated at diferent temperatures: (•) SiO_2

Table 1 The crystallite sizes of $CoFe_2O_4$ (D_1) nanocrystal and silica-coated $CoFe_2O_4$ (D_2) nanocomposite varied with the calcination temperatures

Calcination temperatures	800 °C	900 °C	1,000 °C
D_1 (nm)	28.9	47.3	52.3
D_2 (nm)	30.0	35.5	36.5

Direct particle size observation by means of TEM confirms the estimation of Scherrer's equation. The particle sizes of silica-coated $CoFe_2O_4$ ferrite heat treated at 800 and 1,000 °C, show a mean particle size of 30–40 nm. The silica shell thickness is about 2–3 nm. From Figs. 2(a) and 3(a), the shape of silica shell is similar to sphere, and it is more regular with the increasing calcination temperature. From Figs. 2(b) and 3(b), it can be observed that electronic diffraction photograph of silica-coated cobalt ferrite calcined at 800 and 1,000 °C are circle and dot, respectively. This phenomenon shows that the crystallization of the sample is more complete with the increasing calcination temperature.

Figure 4 shows the IR spectra of the silica-coated cobalt ferrite nanoparticles obtained after thermal treatment at 800, 900 and 1,000 °C for 2 h. IR absorption bands of silica-coated $CoFe_2O_4$ nanoparticles are listed in Table 2. As shown in Fig. 4 and Table 2, for the silica-coated cobalt ferrite calcined at 800 °C, the IR band at 1629.6 cm^{-1} is ascribed to the stretching modes and H–O–H bending vibrations of the free absorbed water. The band at 1087.7, 806.1 and 470.5 cm^{-1} indicate the formation of a silica network [10]. The band at 966.4 cm^{-1} is composed of the contributions from Si–O–H stretching vibrations and from Si–O–Fe vibrations [11]. A faint band at 576.6 cm^{-1} is associated with the Fe–O stretching in Fe–O–Si bonds [12]. This indicates the existence of slight interaction between the $CoFe_2O_4$ nanocrystal and silica shell. For samples obtained at treatment temperatures of 900 and 1,000 °C, the intensity for the broad bands associated with the absorbed water were slightly weakened. The characteristic absorptions for the silica network remained nearly the same as those of sample heat treated at 800 °C. It should be noted that the bands at 966.4 cm^{-1} were disappeared, which could be ascribed to the absence of Si–O–Fe bonds. The results reflect the broken Si–O–Fe bonds, consistent with the disappearance of Fe–O stretching band at ca. 576.6 cm^{-1} for Si–O–Fe bonds. Therefore, the interaction between the $CoFe_2O_4$ nanocrystal and the silica shell became disappearing with the increasing heat treatment temperatures. The absorptions that appeared at ca. 590 cm^{-1} can be

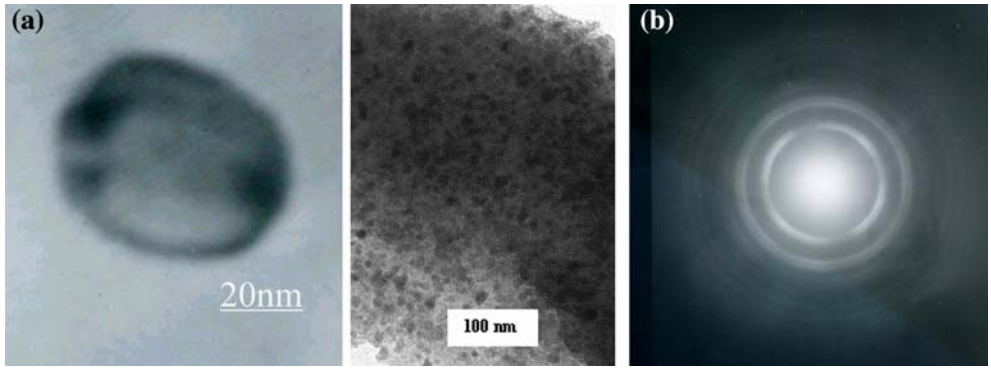

Fig. 2 Transmission electron micrograph images and electronic diffraction photograph for silica-coated $CoFe_2O_4$ calcined at 800 °C (**a**) and (**b**), respectively

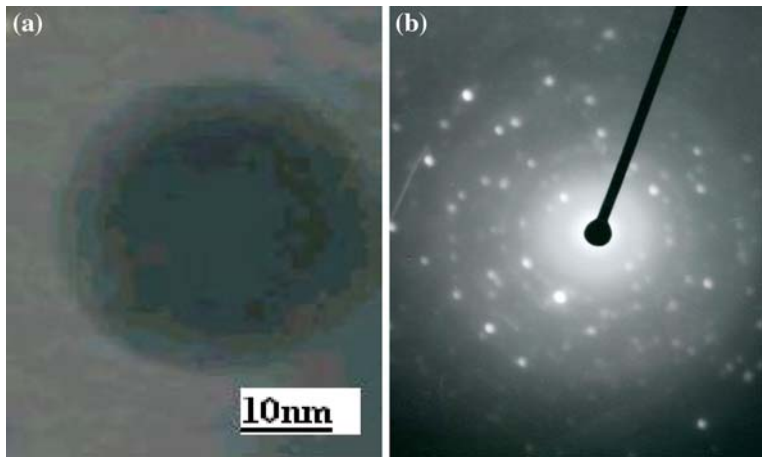

Fig. 3 Transmission electron micrograph images and electronic diffraction photograph for silica-coated $CoFe_2O_4$ calcined at 1,000 °C (**a**) and (**b**), respectively

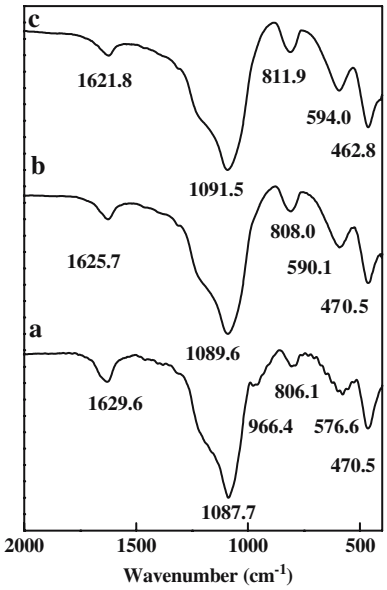

Fig. 4 IR spectra of silica-coated $CoFe_2O_4$ nanocomposite obtained by heat treatment in air at 800 °C (**a**), 900 °C (**b**) and 1,000 °C (**c**)

associated with the characteristic Fe–O stretching modes in $CoFe_2O_4$ phase. The change of bond types of Fe–O–Si to Fe–O–Fe in $CoFe_2O_4$ should reflect the transformation of FO_6 octahedron covalency to FeO_4 tetrahedron accompanied with an enhanced covalency of Fe–O bonding [13].

The magnetic parameters of $CoFe_2O_4$ and silica-coated $CoFe_2O_4$ nanoparticles calcined at different temperatures are listed in Table 3. The saturation magnetization reaches the maximum values for both the $CoFe_2O_4$ and silica-coated $CoFe_2O_4$ nanoparticles calcined at 900 °C. This may be attributed to the complete crystallization of $CoFe_2O_4$ nanoparticles calcined at 900 °C. The presence of non-magnetic iron oxide at higher temperature, i.e., the change of magnetite in hematite, could explain why the magnetization is decreased at 1,000 °C. However, the iron oxide can only be trace quantity, so it cannot be detected from the XRD pattern. Further more, the silica network may also confine the change of magnetite in hematite, the coated silica improves i.e., transformation temperature of the change of magnetitle in hematile. The Ms of coated sample is slightly less than that of uncoated sample, and the Hc of coated sample is significantly larger than that of

Table 2 IR absorption bands of silica-coated $CoFe_2O_4$ calcined at 800 °C (a), 900 °C (b) and 1,000 °C (c)

Sample	Wave number (cm^{-1})						
a	1629.6	1087.7	966.4	806.1	576.6	–	470.5
b	1625.7	1089.6	–	808.0	–	590.1	470.5
c	1621.8	1091.5	–	811.9	–	594.0	462.8

Table 3 The magnetic parameters of silica-coated $CoFe_2O_4$ nanocrystal calcined at different temperatures

Sample	*D* (nm)	Ms (emu/g)	Mr (emu/g)	Hc (Oe)
$CoFe_2O_4$-800 °C	28.9	71.5	27.9	777.5
$CoFe_2O_4/SiO_2$-800 °C	30.0	65.3	28.6	1100.5
$CoFe_2O_4$-900 °C	47.3	76.8	26.9	605.3
$CoFe_2O_4/SiO_2$-900 °C	35.5	66.9	25.6	714.5
$CoFe_2O_4$-1,000 °C	52.3	71.4	24.8	527.5
$CoFe_2O_4/SiO_2$-1,000 °C	36.5	66.0	25.6	703.6

uncoated sample. The above mention can also be observed directly from Fig. 5. This may be due to the formation of non-crystalline silica on the surface of $CoFe_2O_4$ nanoparticles, and the magnetic dilution effect of inert silica restricts the domain wall motion. It is difficult for the silica-coated $CoFe_2O_4$ nanoparticles to move domain walls, because the silica nails and hinders the motion of domain walls. The coercivity is decided by the particle size and thermal treatment. When the particle size is about 30 nm, the Hc of both $CoFe_2O_4$ and silica-coated $CoFe_2O_4$ nanoparticles reached the greatest values. The magnetic properties of a magnetic material depend largely on the particle size distributions as the domain structure and magnetization process depends on particle size [14]. Fig. 6 shows the relation between coercivity and particle size. When the particle size is much larger than the critical size of a single-domain, the coercivity is decided by magnetic displacement, so the value of coercivty is small. When the particle size is reduced to the critical size of single-domain, the coercivity is decided by magnetic domain rotation, so

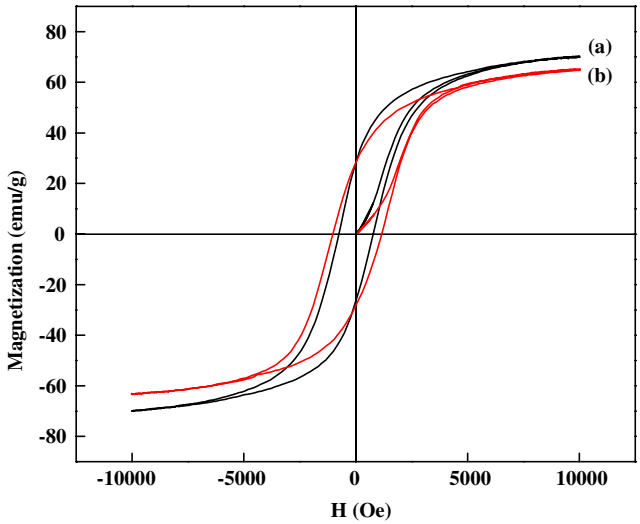

Fig. 5 The hysteresis loop of $CoFe_2O_4$ (**a**) and silica-coated $CoFe_2O_4$ (**b**) nanoparticles calcined at 800 °C

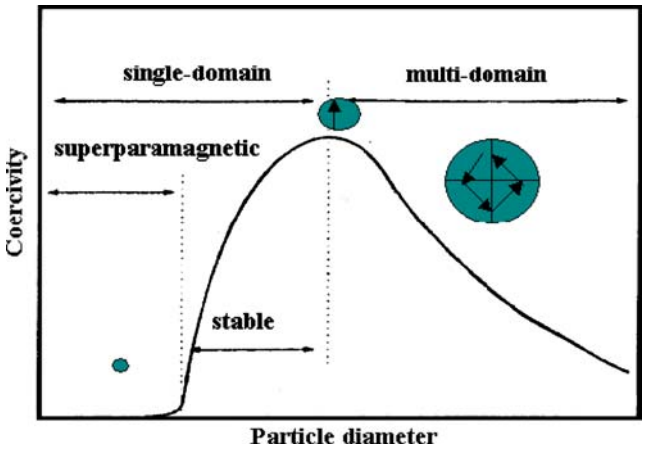

Fig. 6 The relation between coercivity and particle size

the coercivity reaches the maximum. When the particle size is less than the critical size of single-domain, the coercivity will be decreased for the existence of superparamagnetism. As a result of it, the coercivity reaches highest values when the particle size is about 30 nm. Perhaps, for $CoFe_2O_4$ nanoparticles, magnetic single domain behavior is occurring at the crystallite size about 30 nm with a maximum in the coercivity according to a coherent rotation of the magnetization. Smaller and larger crystallite sizes give rise to a decrease in the coercivity due to superparamagnetic and multidomain behavior.

Conclusions

The silica is clearly non-crystalline but short-range correlation results in a very broad peak centered at a low two theta value of 22.5°, even if it is calcined at 1,000 °C. The crystallite sizes of silica-coated $CoFe_2O_4$ ferrite are almost independent of the calcination temperatures. This may be deduced that a well-established silica network provides a more effective confinement to the growth of $CoFe_2O_4$ particles. A silica shell thickness of about 2–3 nm was synthesized on top of cobalt ferrite nanoparticles. Saturation magnetization was decreased slightly and coercivity was increased, when the non-crystalline silica was coated on the surface of cobalt ferrite nanoparticles.

Acknowledgements This work is supported by the National Natural Science Foundation of China (NSFC) (Grant No. 50372025 and 50572033).

References

1. Tsoukatos A, Wan H, Hadjipanayis GC, Papaefthymiou V, Kostikas A, Simopoulos A (1993) J Appl Phys 72:6967
2. Ohmori M, Matijevic E (1992) J Colloid Interface Sci 150:594
3. Ohmori M, Matijevic E (1993) J Colloid Interface Sci 160:288
4. Philipse AP, van Bruggen MPB, Pathmamanoharan C (1994) Langmuir 10:92
5. (a) Kurmoo M (1999) Chem Mater 11:3370; (b) Kurmoo M, Kepert, CJ (1998) New J Chem 1525; (c) Kurmoo M, Kumagai H, Green MA, Lovett BW, Blundell SJ, Ardavan A, Singleton J (2001) J Solid State Chem 159:343
6. Zachariah MR, Shull RD, McMillin BK, Biswas P (1996) In: Chow GM, Gonsaloves KE (eds) Nanotechnology: molecularly designed materials, ACS Symposium Series, vol 622. ACS, Wasgington, p 42
7. Jacobs IS, Bean CP (1963) In: Rado GT, Suhl H (eds) Magnetism, vol 3. Academic Press, NewYork, Ch. 6
8. Anmar S, Helfen A, Jouini N, Fiévet F, Rosenman I, Villain F, Molinié P, Donot M (2001) J Mater Chem 11:186
9. Plocek J, Hutlová A, Nižňanský D, Buršík J, Rehspringer J-L, Mička Z (2003) J Non Cryst Soli 315:70
10. del Monte F, Morales MP, Levy D (1997) Langmuir 13:3627
11. Li G-S, Li L-P, Smith RL Jr, Inomata H (2001) J Mol Struct 560:87
12. Bruni S, Cariati F, Casu M, Lai A, Musinu A, Picccaluga G, Solinas S (1999) Nanostruct Mater 11:573
13. Hui Huang X, Chen Z (2004) J Crystal Growth 271:287
14. Chikazumi S (1964) Physics of magnetism, Wiley, New York, NY, p 411